Nondipole effects and photoelectron momentum shifts in strong-field ionization by infrared light

Morten Førre *

Department of Physics and Technology, University of Bergen, N-5020 Bergen, Norway

(Received 18 January 2022; revised 15 June 2022; accepted 24 June 2022; published 7 July 2022)

High-order above-threshold ionization is studied theoretically beyond the electric dipole approximation. A hydrogen atom is assumed exposed to an ultrashort linearly polarized laser pulse with a central wavelength of 800 nm. The photoelectron momentum distribution from the corresponding nondipole multiphoton ionization process is calculated by means of numerical simulations with the time-dependent Schrödinger equation. In agreement with recent experiments as well as previous theoretical predictions, a forward-backward asymmetry with respect to the light propagation direction is revealed in the resulting momentum spectrum. Investigating separately the role of the linear and quadratic laser-matter interaction terms, i.e., the terms in the system Hamiltonian that are linear and quadratic in the laser's vector potential $\boldsymbol{A}$, respectively, it is found that the linear term introduces a shift of the electron momentum distribution in the laser propagation (forward) direction whereas the quadratic term is responsible for a corresponding backward shift. Nevertheless, only their net effect is observed in the final spectrum, and the quadratic contribution is shown to be responsible for the experimentally observed backward shift of the distribution for small electron momenta. Furthermore, for higher electron momenta it is found that the linear term takes over as the leading source of beyond-dipole ionization, effectively shifting the distribution in the forward direction.

DOI: 10.1103/PhysRevA.106.013104

I. INTRODUCTION

The question of how the nondipole component of a laser field alters the multiphoton ionization of atoms and molecules has become an area of increasing interest [1–14]. Experiments on strong-field ionization of atoms by laser pulses of femtosecond duration in the near- and mid-infrared domain (800–3400 nm) have reported on measurements of characteristic non-dipole-induced photoelectron momentum shifts along the laser propagation direction [15–21]. In the pioneering work of Smeenk *et al.* [15] on single ionization of noble gas atoms by circularly polarized laser fields, a small and positive shift (forward shift) of the momentum distribution with respect to the light propagation direction was observed. Later applying linearly polarized laser pulses instead, Ludwig *et al.* [16] and Maurer *et al.* [17] measured a corresponding negative shift (backward shift) of the position of the peak in the photoelectron momentum distribution. This non-dipole-induced symmetry breaking in the electron's momentum distribution with respect to the beam propagation direction has since been confirmed in various theoretical models and calculations [22–29], and excellent agreement between experimental results and theoretical predictions has been reported [13,20].

In the present paper, developing an *ab initio* model for solving the three-dimensional time-dependent Schrödinger equation beyond the dipole approximation, we revisit the problem of nondipole photoelectron momentum shifts in strong-field ionization. The interaction between a hydrogen atom and an ultrashort linearly polarized Ti:sapphire laser at 800 nm is considered, and the non-dipole-induced forward-backward asymmetry in the photoelectron momentum distribution along the laser's propagation direction is investigated in some detail. An analysis of the relative influence of the linear and quadratic laser-matter interactions on the nondipole ionization reveals that they both contribute equally. The linear and quadratic components are here represented by the $\boldsymbol{A}\cdot\boldsymbol{p}$ and A^2 terms in the system Hamiltonian, respectively, where $\boldsymbol{A}$ is the vector potential defining the laser field. It is also found that the linear term is responsible for an overall shift of the photoelectron momentum distribution in the light propagation direction, whereas the quadratic term, on the other hand, is causing a corresponding shift in the complete opposite direction, i.e., they are both competing against each other, and only their net effect is captured in the final spectra. Furthermore, whereas the quadratic term turns out to be responsible for the observed shift of the peak of the photoelectron momentum spectrum opposite to the beam propagation direction, it is here shown that it is the linear component that gives rise to the net positive shift of the electron's average momentum in the forward direction.

Atomic units (a.u.) are used where stated explicitly.

II. THEORY

A laser field characterized by some angular frequency ω and propagating in the direction given by the wave-vector $\boldsymbol{k}=\omega/c\,\hat{\boldsymbol{k}}$ is conveniently modeled by the vector potential $\boldsymbol{A}(\omega t-\boldsymbol{k}\cdot\boldsymbol{r})$. Here $\hat{\boldsymbol{k}}$ is a unit vector pointing in the laser propagation direction, c is the speed of light, and the Coulomb gauge condition $\nabla\cdot\boldsymbol{A}=0$ is assumed. The vector potential generally depends on both space and time coordinates, but

*morten.forre@uib.no

the spatial degree of freedom may be difficult to handle in actual calculations as it most often leads to a rather involved numerical task. Therefore, in order to simplify the theoretical analysis, the dipole approximation is often used. In this approximation the spatial dependence of the field is not considered, i.e., the vector potential $\boldsymbol{A}$ is assumed to depend on time only. The dipole approximation relies on the assumption that the extension of the quantum system in question is much smaller than the wavelength of the electromagnetic wave hitting it as well as the assumption that the intensity of the radiation is not so high that magnetic-field effects become important.

To account for beyond-dipole (nondipole) effects in the light-matter interaction, it is common to expand the vector potential in terms of a Maclaurin series, i.e., writing

$$\boldsymbol{A}(\omega t - \boldsymbol{k}\cdot\boldsymbol{r}) = \boldsymbol{A}_0 + \frac{\boldsymbol{k}\cdot\boldsymbol{r}}{\omega}\boldsymbol{E}_0 - \frac{1}{2}\left(\frac{\boldsymbol{k}\cdot\boldsymbol{r}}{\omega}\right)^2 \frac{\partial \boldsymbol{E}_0}{\partial t} + \cdots, \quad (1)$$

where the zeroth-order term $\boldsymbol{A}_0 = \boldsymbol{A}_0(\omega t)$ here represents the dipole field and $\boldsymbol{E}_0 = -\frac{\partial}{\partial t}\boldsymbol{A}_0$ is the corresponding electric field. Maintaining only this first term in the Maclaurin series, the magnetic-field $\boldsymbol{B} = \boldsymbol{\nabla}\times\boldsymbol{A}$ cancels, meaning that the magnetic-field component of the radiation is neglected in the dipole approximation. The first- and higher-order terms in expansion (1) account for nondipole corrections, i.e., spatial variations in the electro-magnetic-field as well as magnetic-field effects.

In the standard approach, the coupling between an electron of charge $q = -e$ and mass m confined in some potential V and the electromagnetic field are introduced into the system Hamiltonian by the minimal coupling prescription $\boldsymbol{p} \to \boldsymbol{p} + e\boldsymbol{A}$. The Hamiltonian in the Coulomb gauge then takes the form

$$H = \frac{p^2}{2m} + V + \frac{e}{m}\boldsymbol{A}\cdot\boldsymbol{p} + \frac{e^2}{2m}A^2. \quad (2)$$

Here the cross term which is proportional to $\boldsymbol{A}\cdot\boldsymbol{p}$ is commonly referred to as the linear interaction term, whereas the square term which is proportional to A^2 is usually known as the quadratic interaction. In order to distinguish between pure dipole and beyond-dipole contributions to the laser-matter interaction, respectively, the Hamiltonian (2) may be written out on the following trivially extended form:

$$H = \frac{p^2}{2m} + V + \underbrace{\frac{e}{m}\boldsymbol{A}_0\cdot\boldsymbol{p}}_{\text{(I)}} + \underbrace{\frac{e}{m}(\boldsymbol{A}-\boldsymbol{A}_0)\cdot\boldsymbol{p}}_{\text{(II)}} + \underbrace{\frac{e^2}{2m}A^2}_{\text{(III)}}, \quad (3)$$

where $\boldsymbol{A}_0 = \boldsymbol{A}_0(\omega t)$ and $\boldsymbol{A} = \boldsymbol{A}(\omega t - \boldsymbol{k}\cdot\boldsymbol{r})$ are defined by Eq. (1). Note here that in the dipole approximation limit $\boldsymbol{A} \to \boldsymbol{A}_0$, term (II) vanishes and term (III) becomes a pure time-dependent factor that can effectively be left out, i.e., it is only the dipole term (I) that contributes to the light-matter interaction in this limit—as it should. As such, any non-dipole-field contributions are introduced via the $\boldsymbol{k}\cdot\boldsymbol{r}$ dependency in the terms (II) and (III). In the following we will refer to terms (II) and (III) as the nondipole linear and quadratic terms, respectively.

The so-called *propagation gauge* formulation of the laser-matter interaction has proven to be a particularly advantageous alternative in treating strong-field ionization dynamics beyond the electric dipole approximation [30–35]. In this formulation the Hamiltonian (3) is substituted by

$$H = \frac{p^2}{2m} + V + \underbrace{\frac{e}{m}\boldsymbol{A}_0\cdot\boldsymbol{p}}_{\text{(I)}} + \underbrace{\frac{e}{m}(\boldsymbol{A}-\boldsymbol{A}_0)\cdot\boldsymbol{p}}_{\text{(II)}} + \underbrace{\frac{e^2}{4m^2c}\{A^2, \hat{\boldsymbol{k}}\cdot\boldsymbol{p}\}}_{\text{(III)}}, \quad (4)$$

where curly brackets denote the anticommutator defined by $\{a, b\} = ab + ba$. The anticommutator originates from the fact that A^2 and $\hat{\boldsymbol{k}}\cdot\boldsymbol{p}$ are generally noncommuting operators. For a derivation of Eq. (4) the reader is referred to Ref. [34]. In the same work [34], considering relativistic corrections and imposing a unitary transformation to the system wave function, it was shown that the Hamiltonian (4) can be further transformed into

$$H = \frac{p^2}{2m} + \underbrace{\frac{e}{m}\boldsymbol{A}_0\cdot\boldsymbol{p}}_{\text{(I)}} + \underbrace{V(\boldsymbol{r}+\boldsymbol{\alpha})}_{\text{(II)}} + \underbrace{\frac{e}{2m^2c}\{\hat{\boldsymbol{k}}\cdot\boldsymbol{p}, \boldsymbol{A}\cdot\boldsymbol{p}\}}_{\text{(II)}} + \underbrace{\frac{e^2}{4m^2c}\{A^2, \hat{\boldsymbol{k}}\cdot\boldsymbol{p}\}}_{\text{(III)}}, \quad (5)$$

with

$$\boldsymbol{\alpha} = \frac{e}{m}\int_{-\infty}^{t}(\boldsymbol{A}-\boldsymbol{A}_0)dt'. \quad (6)$$

The Hamiltonian (5) now contains in total three terms that are associated with the beyond-dipole component of the electromagnetic field, i.e., the propagation gauge term (III) from Eq. (4) as well as two new terms which arise from the original term (II) in Eqs. (3) and (4).

In this paper, we will only consider leading order nondipole effects, i.e., corrections of order $1/c$ to the dipole field. To this end, the modified confining potential $V(\boldsymbol{r}+\boldsymbol{\alpha})$ is expanded in powers of $1/c$ writing

$$V(\boldsymbol{r}+\boldsymbol{\alpha}) = V(\boldsymbol{r}) - \frac{e}{mc}(\hat{\boldsymbol{k}}\cdot\boldsymbol{r})(\boldsymbol{\nabla}V\cdot\boldsymbol{A}_0) + \cdots, \quad (7)$$

and where only the first-order correction to the bare (Coulomb) potential is kept in the sequel. Furthermore, the space- and time-dependent vector potential $\boldsymbol{A}(\omega t - \boldsymbol{k}\cdot\boldsymbol{r})$ in the remaining two beyond-dipole interaction terms in (5) is substituted by $\boldsymbol{A}_0(\omega t)$. Then finally the Hamiltonian (5) attains the simpler approximate form

$$H \simeq \frac{p^2}{2m} + V + \underbrace{\frac{e}{m}\boldsymbol{A}_0\cdot\boldsymbol{p}}_{\text{(I)}} + \underbrace{\frac{e}{m^2c}(\hat{\boldsymbol{k}}\cdot\boldsymbol{p})(\boldsymbol{A}_0\cdot\boldsymbol{p})}_{\text{(II)}} - \underbrace{\frac{e}{mc}(\hat{\boldsymbol{k}}\cdot\boldsymbol{r})(\boldsymbol{\nabla}V\cdot\boldsymbol{A}_0)}_{\text{(II)}} + \underbrace{\frac{e^2}{2m^2c}A_0^2\hat{\boldsymbol{k}}\cdot\boldsymbol{p}}_{\text{(III)}}, \quad (8)$$

where $V = V(\boldsymbol{r})$ now refers to the unshifted potential and where all terms of order $1/c^2$ and higher have been left out. Note that the anticommutation rules of Eq. (5) become unnecessary as $\boldsymbol{A} \to \boldsymbol{A}_0$ since the operators now commute, and they have, therefore, been omitted in the final result. The relative role of the nondipole terms (II) and (III) for multiphoton ionization processes induced by intense xuv and x-ray laser fields was investigated in Refs. [9,36], and it was concluded

that the quadratic term (III) is by far the most important one. In stark contrast to this conclusion for high-frequency fields, in the present paper it will become evident that both terms (II) and (III) are equally important when it comes to strong-field ionization by low-frequency (infrared) light.

The Hamiltonian (8) is the base for the present theoretical analysis of the hydrogen atom interacting with a near-infrared 800-nm laser pulse. The reason why this particular formulation is chosen in the present paper is that this representation of the light-matter interaction has proven to be very favorable from the numerical point of view, in particular, in the limit of very strong perturbations [34]. The atom is assumed being exposed to a linearly (z) polarized laser field which is propagating in the positive x direction, i.e., $\boldsymbol{A}_0(t) = A_0(t)\hat{\boldsymbol{z}}$, $\hat{\boldsymbol{k}} \cdot \boldsymbol{r} = x$ and $\hat{\boldsymbol{k}} \cdot \boldsymbol{p} = p_x$ in Eq. (8). Furthermore, the temporal evolution $A_0(t)$ of the field is given by

$$A_0(t) = \frac{E_0}{\omega} f(t) \sin(\omega t + \phi), \tag{9}$$

where E_0 is the electric-field strength at peak intensity, ϕ is the carrier-envelope phase (CEP) and where $f(t)$ defines the temporal shape of the pulse,

$$f(t) = \begin{cases} \sin^2\left(\frac{\pi t}{T}\right), & 0 < t < T, \\ 0, & \text{otherwise}, \end{cases} \tag{10}$$

T being the total duration. In this paper, the pulse duration is fixed at three cycles, i.e., $T = 3\times 2\pi/\omega \simeq 8.00$ fs. For such short pulses the value of the CEP may play some role in the interaction, and, therefore, two different values for the CEP $\phi = 0$ and $\phi = \pi/2$ are considered.

The evolution in time of the wave-function $\Psi(\boldsymbol{r}, t)$ for the hydrogen electron interacting with the electromagnetic field is governed by the time-dependent Schrödinger equation (TDSE),

$$i\hbar \frac{\partial}{\partial t} \Psi = H\Psi. \tag{11}$$

The TDSE is here discretized by expanding the solution $\Psi(\boldsymbol{r}, t)$ on products of hydrogenic radial wave functions and spherical harmonics. The radial wave functions are calculated numerically on a grid by solving the corresponding eigenvalue problem for the field-free (static) atomic Hamiltonian in a B-spline basis [37]. The matrix elements of the light-matter coupling matrix (8) are then computed, and the resulting system of ordinary differential equations is solved by a predictor-corrector method developed by Gordon and Shampine [38]. For laser intensities up to $I_0 = 5\times 10^{14}$ W/cm^2, accurate numerical results were obtained with a radial grid extending to $r = |\boldsymbol{r}| = 900$ a.u. and with the maximum allowable kinetic energy of the (field-free) electron set to 15 a.u. Furthermore, the number of angular momentum pairs (l, m) included in the expansion of the wave function was increased until satisfactory convergence of the calculations was achieved. As it turned out, for the azimuthal quantum number l the values $l = 0, 1, 2, \ldots, 60$ were necessary, whereas for the magnetic quantum number m the values of $m = -2, -1, 0, 1, 2$ were sufficed. For the interested reader, more details on the numerical methods employed in the present paper in order to solve the TDSE and extract information on physical observables from the system wave function are given in Refs. [9,32,34,36].

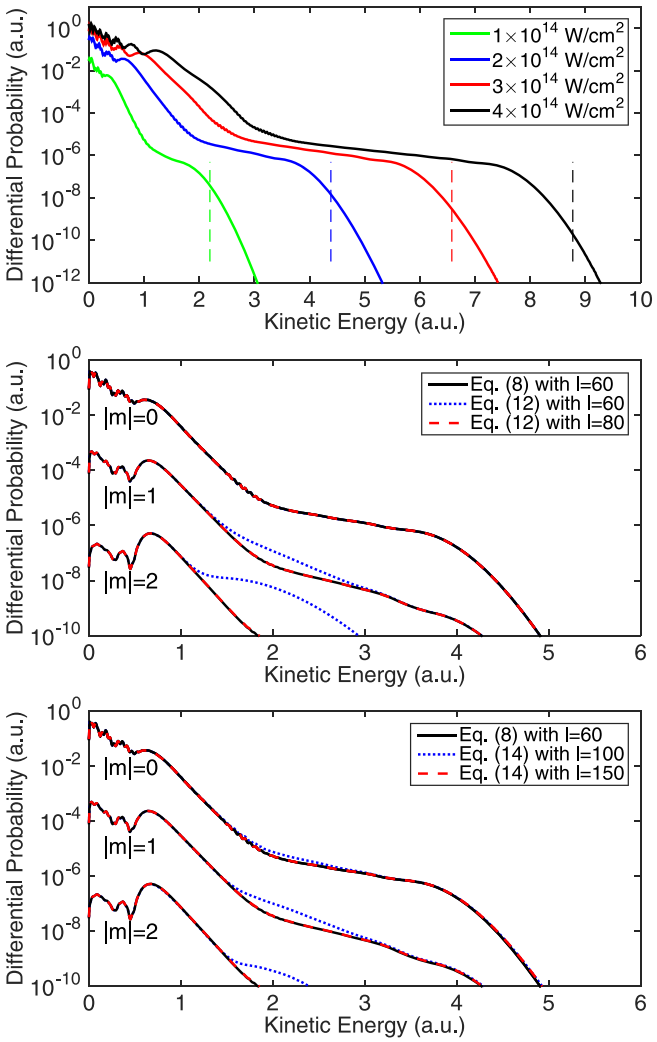

FIG. 1. (Top panel) Converged (nondipole) kinetic-energy spectra of the emitted photoelectron as obtained for a linearly polarized three-cycle 800-nm laser pulse of intensities 1×10^{14} W/cm^2 (green left line), 2×10^{14} W/cm^2 (blue line second from left), 3×10^{14} W/cm^2 (red line third from left), and 4×10^{14} W/cm^2 (black right line). The CEP in Eq. (9) is set to zero in all cases. The 10-U_p cutoff is in each case indicated with a dashed line in the figure, U_p being the ponderomotive energy. (Middle and bottom panels) Partial contribution from the $|m| = 0$ (dipole), $|m| = 1$ (nondipole), and $|m| = 2$ (nondipole) channels to the total energy spectrum for the laser intensity 2×10^{14} W/cm^2. Black lines in each panel represent the reference (converged) data as obtained with the Hamiltonian (8) and with the maximum allowable value of the angular momentum quantum number l set to 60. Blue dotted and red dashed lines in the middle panel depict the corresponding result obtained with the Hamiltonian (12) setting the maximum value for $l = 60$ and 80, respectively. Likewise, blue dotted and red dashed lines in the bottom panel depict the result obtained with the Hamiltonian (14) setting the maximum value for $l = 100$ and 150, respectively.

The upper panel in Fig. 1 shows converged photoelectron energy distributions for four different values of the laser intensity, i.e., from left to right 1–3 and 4×10^{14} W/cm^2,

respectively. Note that as far as the total photoelectron spectrum is concerned, both the dipole and the nondipole spectra are virtually identical and could not be distinguished on the axis scale of the figure. The solid black lines in the middle and bottom panels depict the contributions from the $m = 0$, $|m| = 1$, and $|m| = 2$ channels to the total energy spectrum for the intensity 2×10^{14} W/cm^2, again as obtained with the Hamiltonian (8). Here, the $|m| = 1$ and 2 represent the leading nondipole corrections to the total ($m = 0$) dipole spectrum. Due to the logarithmic scale it becomes clear that nondipole corrections are generally small as far as the total energy distribution is concerned. However, as will be demonstrated in the Results section, nondipole effects will nevertheless induce a non-negligible shift of the photoelectron momentum distribution, a shift that has already been measured experimentally.

As an extra check of the validity of the calculations as well as demonstrating the efficiency of the here chosen light-matter interaction form (8), additional test calculations using two alternative interaction forms were executed, i.e., a beyond-dipole generalization of the common length gauge formulation as well as applying the minimal coupling Hamiltonian (2) directly in its present form but expanding the vector potential as in Eq. (1) and keeping only terms up to (and including) the $1/c$ beyond-dipole corrections. The minimal coupling Hamiltonian then takes the approximate form

$$H \simeq \frac{p^2}{2m} + V + \underbrace{\frac{e}{m}\boldsymbol{A}_0 \cdot \boldsymbol{p}}_{\text{(II)}} + \underbrace{\frac{e}{mc}(\hat{\boldsymbol{k}} \cdot \boldsymbol{r})\, \boldsymbol{E}_0 \cdot \boldsymbol{p}}_{\text{(III)}} + \underbrace{\frac{e^2}{mc}(\hat{\boldsymbol{k}} \cdot \boldsymbol{r})\boldsymbol{A}_0 \cdot \boldsymbol{E}_0}_{\text{(III)}} + \underbrace{\frac{e^2}{2m}A_0^2}_{\text{(III)}}. \tag{12}$$

Note here that the last term is purely time dependent and may be omitted in the numerical analysis. Furthermore, note that there is a one-to-one correspondence between terms (II) and (III) in the Hamiltonians (8) and (12), respectively, i.e., this splitting into terms (II) and (III) is invariant to the unitary transformation relating the two Hamiltonians. The nondipole length gauge formulation of the interaction is obtained by introducing the gauge (unitary) transformation,

$$\begin{aligned} \boldsymbol{A}_0 &\to \boldsymbol{A}_0 + \boldsymbol{\nabla} f, \\ V &\to V + e\frac{\partial f}{\partial t}, \\ \Psi'(\boldsymbol{r}, t) &= e^{-ief(\boldsymbol{r},t)/\hbar}\Psi(\boldsymbol{r}, t), \end{aligned} \tag{13}$$

and simply choosing $f(\boldsymbol{r}, t) = -\boldsymbol{A}_0 \cdot \boldsymbol{r}$. Then the Hamiltonian (12) transforms into

$$H \simeq \frac{p^2}{2m} + V + e\boldsymbol{E}_0 \cdot \boldsymbol{r} + \frac{e}{mc}(\hat{\boldsymbol{k}} \cdot \boldsymbol{r})\, \boldsymbol{E}_0 \cdot \boldsymbol{p}. \tag{14}$$

The dashed red and dotted blue lines in the middle panel of Fig. 1 show the energy distribution obtained when applying the Hamiltonian (12) and setting the maximum allowable l value in the wave-function expansion to 60 (dotted blue line) and 80 (dashed red line), respectively. Likewise, the bottom panel depicts the results obtained with the Hamiltonian (14) and choosing the maximum allowable l value equal 100 (dotted blue line) and 150 (dashed red line), respectively. In each case, the corresponding reference data obtained with the Hamiltonian (8) and with the maximum allowable l set to 60 are shown for comparison. (It is here worth noting that choosing maximum $l = 50$ would suffice in this case). Thus, as it turns out, both Hamiltonians (12) and (14) require a higher number of basis functions in order to produce converged results as compared to the formulation (8), the nondipole length gauge formulation being the most slowly converging representation. Note that this comparison has been performed at a relatively moderate laser intensity of 2×10^{14} W/cm^2 and that even greater differences in numerical performances are expected at higher intensities. This behavior, when it comes to the rate of convergence with respect to basis size, is in concordance the previous studies outlined for higher laser frequencies [30–35]. We may, therefore, conclude that the laser-matter representation (8) is beneficial for modeling strong-field nondipole ionization processes not only in the high-frequency regime, but also for low-frequency fields.

III. RESULTS AND DISCUSSION

Figure 2 shows the transverse electron momentum distribution, which describes the probability density for detecting an ionized electron with a given value of the momentum along the laser propagation direction, i.e., perpendicular to the polarization plane of the laser field. The distribution is obtained for a linearly polarized three-cycle 800-nm laser pulse of intensity $I = 4\times10^{14}$ W/cm^2 setting the carrier-envelope phase to zero in Eq. (9). The light is assumed to propagate in the positive x direction as indicated by the arrow in the figure. The resulting spectrum has been integrated over all values of p_y and p_z, where p_z is the momentum component along the electric-field polarization axis, i.e., the longitudinal electron momentum. The first (top) panel shows a comparison of the result obtained with the full beyond-dipole Hamiltonian (8) (solid black line) and the corresponding result using the dipole approximation (dashed red line). The left inset in the figure shows a zoom of the spectrum around the peak value corresponding to low transverse momentum values. Likewise the right inset shows a zoom at higher transverse momentum values. The figure reveals two characteristic features of the ionization: First the peak of the distribution is shifted towards negative values of the momentum, i.e., electrons characterized by very low-momentum components along the laser's propagation (transverse) direction are likely to receive a net momentum kick in the counterpropagating direction due to the nondipole interaction with the laser field, and second the distribution is shifted towards positive momentum transfers for electrons with larger transverse momentum components. Both these two findings are in concordance with previous studies, see, e.g., Refs. [13,20,22,25] and references therein.

The second panel in Fig. 2 again shows a comparison of the dipole approximation calculation and the full nondipole calculation as obtained for a limited range of transverse momentum values around the peak. Albeit still small relative to the chosen scale of the figure, both the shift of the peak position and the overall positive shift of the distribution at larger momentum transfers may yet be identified in the figure. The third panel in Fig. 2 shows the corresponding result obtained when only the nondipole linear term (II) is taken into account in the calculation (solid black line), i.e., when term (III) is excluded

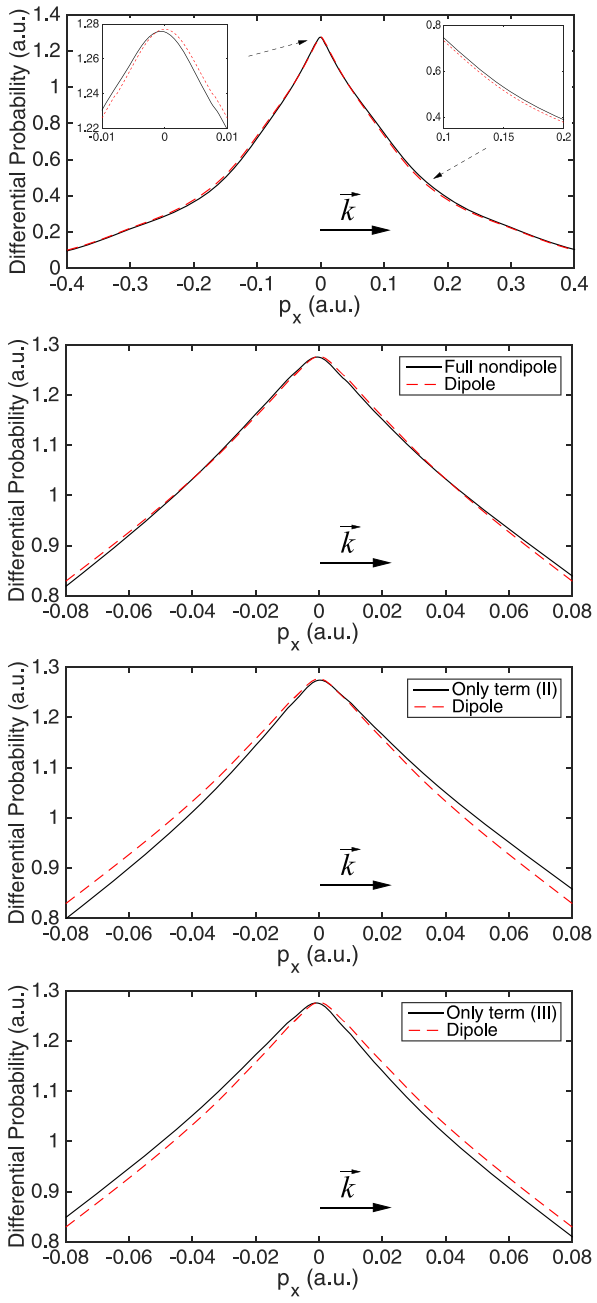

FIG. 2. Transverse electron momentum distribution along the laser propagation axis (i.e., the x axis) as obtained by integrating over both p_y and p_z, respectively. The atom is assumed irradiated by a linearly polarized three-cycle 800-nm laser pulse of intensity $I = 4\times10^{14}$ W/cm^2 choosing the CEP $\phi = 0$ in Eq. (9). (Two upper panels) The full nondipole result as obtained with the Hamiltonian (8) including both the beyond-dipole linear (II) and the quadratic (III) contributions (solid black line). (Third panel) The corresponding result obtained with the nondipole linear term (II) solely (solid black line). (Bottom panel) The corresponding result obtained with the nondipole quadratic term (III) solely (solid black line). In all panels dashed red lines are the corresponding dipole approximation result. In the full nondipole calculation including both terms (II) and (III), the central peak is shifted by -0.0006 a.u. with respect to the dipole approximation result, whereas the corresponding shifts are $+0.0003$ and -0.0009 a.u. when only term (II) or (III) is taken into account, respectively.

from the Hamiltonian (8). Again the dipole approximation result is shown as a dashed red line. Likewise the bottom panel shows a comparison between the dipole result (dashed red line) and the result obtained with only the nondipole quadratic term (III) included (solid black line). In this last case the nondipole linear term (II) has been omitted in the calculation. From these comparisons it becomes evident that the nondipole linear term generally induces an overall positive (forward) shift of the photoelectron momentum distribution in the beam propagation direction, whereas the quadratic term is responsible for a corresponding shift in the negative (backward) direction. Furthermore, the two shifts are of comparable size, merely illustrating that both nondipole contributions are important and cannot be neglected in the theoretical analysis. Computing the algebraic mean of the two distributions the positive and negative shifts tend to cancel each other out. Notwithstanding the comparison between the full spectrum and its dipole counterpart in the two upper panels in Fig. 2 clearly reveals that the cancellation is not exact, i.e., a negative shift of the peak position of the distribution by -0.0006 a.u. as well as an overall positive shift of the momentum at higher momentum transfers are ultimately manifested in the total spectrum. Based on the present findings we may now conclude that it is the quadratic term that is responsible for the backward shift of the position of the peak, but it is the linear term that generally causes the overall positive shift of the distribution at higher electron momenta.

The dependence of the photoelectron momentum shifts on the laser intensity is investigated further in Fig. 3. Two different values for the carrier-envelope phase $\phi = 0$ and $\phi = \pi/2$ are considered. The top panel in the figure shows the expectation value of the electron momentum $\langle p_x \rangle$ along the laser propagation axis as a function of the intensity of the applied laser field. The bottom panel depicts the corresponding shift of the peak in the photoelectron momentum distribution. As seen in the figure, the mean value of the electron's momentum along the laser beam direction is found to be a positive and monotonically increasing function over the whole intensity region considered. Furthermore, the (negative) shift of the peak position is found to become more and more prominent with increasing laser intensity. As it turns out, the value of the CEP does not appear to affect the results any significantly despite the relatively short pulse considered.

In order to disentangle the relative importance of the linear (II) and quadratic (III) nondipole terms on the shifting of the spectra for different laser intensities, Fig. 4 shows a comparison between the linear and the quadratic contributions, respectively, and the full nondipole result. From these results it becomes even more evident that it is the quadratic term (III) that is the main contributor to the observed negative shift of the position of the peak. As a matter fact if the quadratic term would have been left out from the simulation, the remaining linear term (II) would have predicted a false positive result for the peak shift for all the laser intensities considered. Likewise if the linear nondipole term in turn is left out, then the remaining quadratic term would have suggested a corresponding erroneous negative result for the average momentum of the emitted photoelectron. Thus, it is of substantial importance to consider both the interactions (II) and (III) in the Hamiltonian (8) in a proper theoretical treatment of the

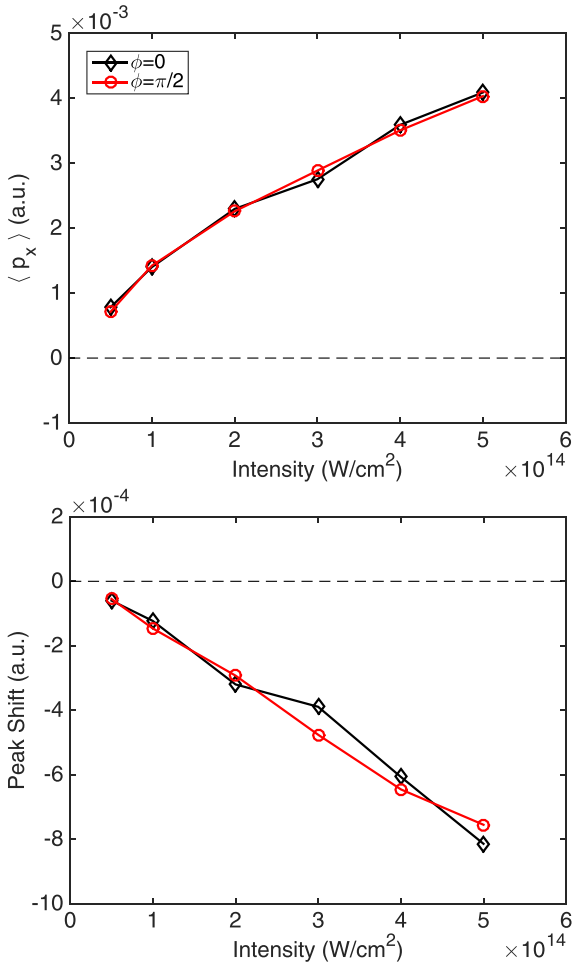

FIG. 3. Top panel: Expectation value of the electron momentum $\langle p_x \rangle$ along the laser propagation axis (i.e., the x axis) as a function of the intensity of the applied laser field. Bottom panel: Shift in the position of the peak (cusp) in the transverse electron momentum distribution along the laser propagation axis (cf. Fig. 2) as a function of the intensity of the laser field. Black lines with diamonds and red lines with circles are results obtained with $\phi = 0$ and $\phi = \pi/2$ in Eq. (9), respectively.

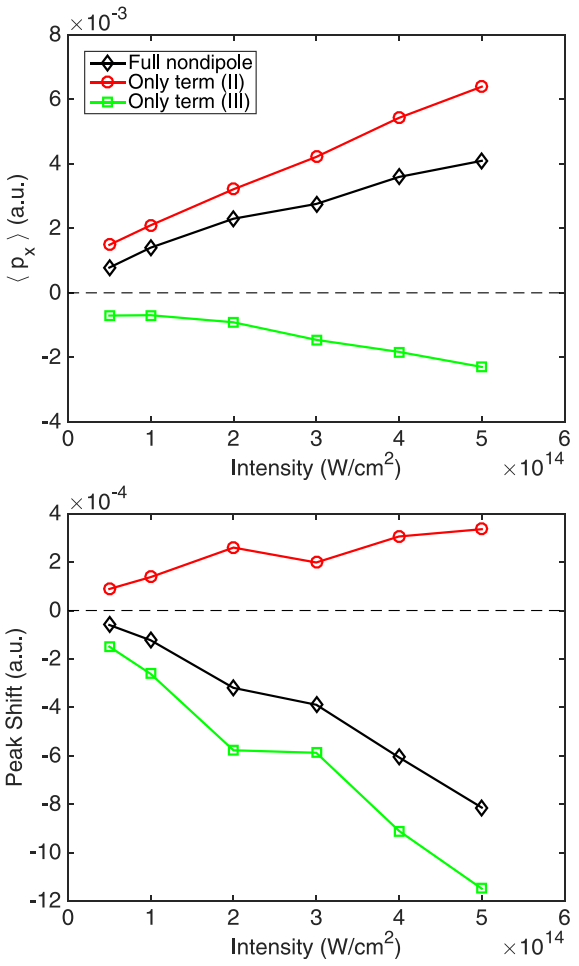

FIG. 4. Top panel: Expectation value of the electron momentum $\langle p_x \rangle$ along the laser propagation axis (i.e., the x axis) as a function of the intensity of the applied laser field. Bottom panel: Shift in the position of the peak (cusp) in the transverse electron momentum distribution along the laser propagation axis (cf. Fig. 2) as a function of the intensity of the laser field. (Black lines with diamonds) The full nondipole result as obtained with the Hamiltonian (8) including both the beyond-dipole linear (II) and the quadratic (III) terms. (Red lines with circles) The corresponding result obtained with the nondipole linear term (II) solely. (Green lines with squares) The corresponding result obtained with the nondipole quadratic term (III) solely. All results are obtained setting $\phi = 0$ in Eq. (9).

beyond-dipole strong-field ionization by infrared light. This conclusion stands in stark contrast to the results of the studies of nondipole multiphoton ionization conducted in the xuv and x-ray regimes [9,36] where it was explicitly demonstrated that the quadratic term (III) is by far the dominating one at intense fields.

IV. CONCLUSION

In conclusion, developing an *ab initio* numerical model we have studied theoretically the photoelectron momentum distributions accompanying the strong-field ionization by linearly polarized 800-nm laser pulses. Focus has been set on the role of the nondipole component of the laser field and its impact on the electron's momentum in the final state. A non-dipole-induced forward-backward asymmetry is identified in the corresponding transverse electron momentum distributions along the laser-beam propagation direction. Investigating separately the role of the linear and quadratic terms on the observed nondipole asymmetries as represented by the $\boldsymbol{A} \cdot \boldsymbol{p}$ and A^2 operators in the initial Hamiltonian (2), respectively, it is found that they are both important for a correct description of the beyond-dipole ionization dynamics. It is also shown that the linear term is generally responsible for a positive non-dipole-induced shift of the photoelectron momentum distribution in the light propagation direction, whereas the quadratic term, on the other hand, is responsible for a corresponding negative shift. Ultimately only their net effect is unveiled in the total spectrum, which exhibits a negative shift at low values of the electron's transverse momentum (due to the quadratic term) and a positive shift at higher values of the momentum (due to the linear term).

As a final remark we would like to add that a very similar negative bias in the corresponding emission spectrum of low-momentum photoelectrons was previously identified also in the xuv nondipole ionization regime at very intense laser fields [5,9,10]. Furthermore, also in that case the quadratic term was found to be responsible for the ionization in the direction opposite to the laser propagation direction, and a mechanism for the observed features was suggested [5].

[1] M. Ilchen, G. Hartmann, E. V. Gryzlova, A. Achner, E. Allaria, A. Beckmann, M. Braune, J. Buck, C. Callegari, R. N. Coffee *et al.*, Nat. Commun. **9**, 4659 (2018).

[2] H. Zimmermann, S. Meise, A. Khujakulov, A. Magaña, A. Saenz, and U. Eichmann, Phys. Rev. Lett. **120**, 123202 (2018).

[3] S. Eilzer, H. Zimmermann, and U. Eichmann, Phys. Rev. Lett. **112**, 113001 (2014).

[4] O. Hemmers, R. Guillemin, E. P. Kanter, B. Krässig, D. W. Lindle, S. H. Southworth, R. Wehlitz, J. Baker, A. Hudson, M. Lotrakul, D. Rolles, W. C. Stolte, I. C. Tran, A. Wolska, S. W. Yu, M. Ya. Amusia, K. T. Cheng, L. V. Chernysheva, W. R. Johnson, and S. T. Manson, Phys. Rev. Lett. **91**, 053002 (2003).

[5] M. Førre, J. P. Hansen, L. Kocbach, S. Selstø, and L. B. Madsen, Phys. Rev. Lett. **97**, 043601 (2006).

[6] H. Bachau, M. Dondera, and V. Florescu, Phys. Rev. Lett. **112**, 073001 (2014).

[7] S. Chelkowski, A. D. Bandrauk, and P. B. Corkum, Phys. Rev. Lett. **113**, 263005 (2014).

[8] N. J. Kylstra, R. A. Worthington, A. Patel, P. L. Knight, J. R. Vázquez de Aldana, and L. Roso, Phys. Rev. Lett. **85**, 1835 (2000).

[9] M. Førre and A. S. Simonsen, Phys. Rev. A **90**, 053411 (2014).

[10] M. Førre, S. Selstø, J. P. Hansen, T. K. Kjeldsen, and L. B. Madsen, Phys. Rev. A **76**, 033415 (2007).

[11] M. Førre, S. Selstø, J. P. Hansen, and L. B. Madsen, Phys. Rev. Lett. **95**, 043601 (2005).

[12] M.-X. Wang, S.-G. Chen, H. Liang, and L.-Y. Peng, Chin. Phys. B **29**, 013302 (2020).

[13] N. Haram, R. T. Sang, and I. V. Litvinyuk, J. Phys. B: At. Mol. Opt. Phys. **53**, 154005 (2020).

[14] J. Maurer and U. Keller, J. Phys. B: At., Mol. Opt. Phys. **54**, 094001 (2021).

[15] C. T. L. Smeenk, L. Arissian, B. Zhou, A. Mysyrowicz, D. M. Villeneuve, A. Staudte, and P. B. Corkum, Phys. Rev. Lett. **106**, 193002 (2011).

[16] A. Ludwig, J. Maurer, B. W. Mayer, C. R. Phillips, L. Gallmann, and U. Keller, Phys. Rev. Lett. **113**, 243001 (2014).

[17] J. Maurer, B. Willenberg, J. Daněk, B. W. Mayer, C. R. Phillips, L. Gallmann, M. Klaiber, K. Z. Hatsagortsyan, C. H. Keitel, and U. Keller, Phys. Rev. A **97**, 013404 (2018).

[18] A. Hartung, S. Brennecke, K. Lin, D. Trabert, K. Fehre, J. Rist, M. S. Schöffler, T. Jahnke, L. Ph. H. Schmidt, M. Kunitski, M. Lein, R. Dörner, and S. Eckart, Phys. Rev. Lett. **126**, 053202 (2021).

[19] A. Hartung, S. Eckart, S. Brennecke, J. Rist, D. Trabert, K. Fehre, M. Richter, H. Sann, S. Zeller, K. Henrichs *et al.*, Nat. Phys. **15**, 1222 (2019).

[20] N. Haram, I. Ivanov, H. Xu, K. T. Kim, A. Atia-tul-Noor, U. S. Sainadh, R. D. Glover, D. Chetty, I. V. Litvinyuk, and R. T. Sang, Phys. Rev. Lett. **123**, 093201 (2019).

[21] B. Willenberg, J. Maurer, B. W. Mayer, and U. Keller, Nat. Commun. **10**, 5548 (2019).

[22] S. Chelkowski, A. D. Bandrauk, and P. B. Corkum, Phys. Rev. A **92**, 051401(R) (2015).

[23] S. Brennecke and M. Lein, J. Phys. B: At. Mol. Opt. Phys. **51**, 094005 (2018).

[24] I. A. Ivanov, Phys. Rev. A **91**, 043410 (2015).

[25] I. A. Ivanov, J. Dubau, and K. T. Kim, Phys. Rev. A **94**, 033405 (2016).

[26] H. Ni, S. Brennecke, X. Gao, P.-L. He, S. Donsa, I. Březinová, F. He, J. Wu, M. Lein, X.-M. Tong, and J. Burgdörfer, Phys. Rev. Lett. **125**, 073202 (2020).

[27] P.-L. He, D. Lao, and F. He, Phys. Rev. Lett. **118**, 163203 (2017).

[28] J. Liu, Q. Z. Xia, J. F. Tao, and L. B. Fu, Phys. Rev. A **87**, 041403(R) (2013).

[29] J. F. Tao, Q. Z. Xia, J. Cai, L. B. Fu, and J. Liu, Phys. Rev. A **95**, 011402(R) (2017).

[30] M. Førre and A. S. Simonsen, Phys. Rev. A **93**, 013423 (2016).

[31] T. K. Lindblom, M. Førre, E. Lindroth, and S. Selstø, Phys. Rev. Lett. **121**, 253202 (2018).

[32] M. Førre, Phys. Rev. A **99**, 053410 (2019).

[33] A. S. Simonsen and M. Førre, Phys. Rev. A **93**, 063425 (2016).

[34] M. Førre and S. Selstø, Phys. Rev. A **101**, 063416 (2020).

[35] T. Kjellsson, M. Førre, A. S. Simonsen, S. Selstø, and E. Lindroth, Phys. Rev. A **96**, 023426 (2017).

[36] T. E. Moe and M. Førre, Phys. Rev. A **97**, 013415 (2018).

[37] H. Bachau, E. Cormier, P. Decleva, J. E. Hansen, and F. Martín, Rep. Prog. Phys. **64**, 1815 (2001).

[38] M. K. Gordon and L. F. Shampine, in *Proceedings of the 1974 Annual Conference ACM '74* (ACM Press, New York, 1974), Vol. 1, pp. 46–53.